Charge-altering releasable transporters (CARTs) for the delivery and release of mRNA in living animals

Colin J. McKinlay[a,1], Jessica R. Vargas[a,1], Timothy R. Blake[a], Jonathan W. Hardy[b,c], Masamitsu Kanada[b,c], Christopher H. Contag[b,c,d,e,f,2], Paul A. Wender[a,g,2], and Robert M. Waymouth[a,2]

[a]Department of Chemistry, Stanford University, Stanford, CA 94305; [b]Department of Pediatrics, Stanford University, Stanford, CA 94305; [c]Molecular Imaging Program at Stanford, Stanford University, Stanford, CA 94305; [d]Department of Microbiology & Immunology, Stanford University, Stanford, CA 94305; [e]Department of Bioengineering, Stanford University, Stanford, CA 94305; [f]Department of Radiology, Stanford University, Stanford, CA 94305; and [g]Department of Chemical and Systems Biology, Stanford University, Stanford, CA 94305

Edited by Daniel G. Anderson, Massachusetts Institute of Technology, Cambridge, MA, and accepted by Editorial Board Member David A. Tirrell December 13, 2016 (received for review August 26, 2016)

Functional delivery of mRNA to tissues in the body is key to implementing fundamentally new and potentially transformative strategies for vaccination, protein replacement therapy, and genome editing, collectively affecting approaches for the prevention, detection, and treatment of disease. Broadly applicable tools for the efficient delivery of mRNA into cultured cells would advance many areas of research, and effective and safe in vivo mRNA delivery could fundamentally transform clinical practice. Here we report the step-economical synthesis and evaluation of a tunable and effective class of synthetic biodegradable materials: charge-altering releasable transporters (CARTs) for mRNA delivery into cells. CARTs are structurally unique and operate through an unprecedented mechanism, serving initially as oligo(α-amino ester) cations that complex, protect, and deliver mRNA and then change physical properties through a degradative, charge-neutralizing intramolecular rearrangement, leading to intracellular release of functional mRNA and highly efficient protein translation. With demonstrated utility in both cultured cells and animals, this mRNA delivery technology should be broadly applicable to numerous research and therapeutic applications.

cell-penetrating | gene therapy | nanoparticle | organocatalysis | stimuli-responsive

Messenger RNA (mRNA) is the template for the synthesis of proteins. Tools for effective transfer of exogenous mRNA into cells in the body would advance a rapidly emerging class of gene therapy drugs with the potential to transform the treatment of illnesses as diverse as cancer, genetic disorders, and infectious diseases (1, 2). Delivery and subsequent expression of mRNA into its encoded protein can be leveraged for a wide range of research, imaging, and therapeutic applications including protein replacement or augmentation therapy and new vaccine strategies either for prophylactic or immunotherapeutic approaches (3–7). Although gene transfer studies of other oligonucleotides such as plasmid DNA and siRNA have dominated the gene delivery field for some time (8–13), the use of mRNA to generate therapeutic proteins has received attention only recently (1, 14–16).

The key challenge associated with the use of therapeutic mRNA is an inability to efficiently deliver functionally intact mRNA into cells. Like all nucleic acid-based drugs, mRNA is a large polyanion and thus it does not readily cross nonpolar cellular and tissue barriers. Moreover, it is also susceptible to rapid degradation by nucleases and so it must be protected during the delivery process (17). Finally, after cell entry, its rapid release in the cytosol and appropriate association with the protein synthesis apparatus is required for translation; each of these is a potential point of failure for functional mRNA delivery (2). In addition to the challenges associated with complexation, protection, delivery, and release, an ideal delivery system would also need to be synthetically accessible, readily tuned for optimal efficacy, and safe.

Despite this being a rapidly emerging subject of intense interest, relatively few classes of materials have been evaluated as mRNA delivery vehicles (14, 18). Those that have emerged are largely inspired by or directly repurposed from DNA and siRNA delivery methods. However, multiple groups have observed that directly adapting DNA or siRNA vehicles to mRNA delivery can be ineffective, and in those cases it has been suggested that insufficient mRNA release from the carrier likely contributes to the observed failed or inefficient delivery (19–23). Nonetheless, there have been encouraging preliminary results of recent and ongoing clinical trials using mRNA, underscoring the rapidly emerging importance of mRNA therapeutics in the treatment or prevention of a range of diseases. To date, naked, chemically modified, or protamine-complexed mRNA have shown promise in phase I/II cancer trials (24–26). Recently, preclinical development of materials specific for mRNA delivery has resulted in cationic polymers such as polymethacrylates (27–29), poly(aspartamides) (30, 31), and polypeptides (32), as well as multicomponent cationic lipid or lipid-like formulations (21, 33–36). In many of these examples, however, transfection efficiencies can be quite low, ranging 20–80% in cells (18), with likely much lower efficiencies in vivo, which requires either high mRNA doses or hydrodynamic injections (32, 37).

Here, we report a highly effective mRNA delivery system comprising charge-altering releasable transporters (CARTs),

Significance

Protein expression using mRNA has the potential to transform many areas of life science research and affect the prevention, detection, and treatment of disease. However, realizing this potential requires the development of readily accessible, efficacious, and safe delivery systems that can functionally deliver mRNA to cells in culture and in vivo. A class of materials developed for mRNA delivery is described that operates through an unprecedented self-immolation mechanism. These materials are accessed in two steps through an organocatalytic oligomerization. They noncovalently complex, protect, deliver, and release mRNA with >99% transfection efficiency in cultured cells and with robust protein expression in mice using multiple routes of administration. This mRNA delivery technology should be broadly applicable to numerous research and therapeutic applications.

Author contributions: C.J.M., J.R.V., T.R.B., J.W.H., M.K., C.H.C., P.A.W., and R.M.W. designed research; C.J.M., J.R.V., T.R.B., J.W.H., and M.K. performed research; C.J.M., J.R.V., T.R.B., J.W.H., M.K., C.H.C., P.A.W., and R.M.W. analyzed data; and C.J.M., J.R.V., T.R.B., P.A.W., and R.M.W. wrote the paper.

The authors declare no conflict of interest.

This article is a PNAS Direct Submission. D.G.A. is a Guest Editor invited by the Editorial Board.

[1]C.J.M. and J.R.V. contributed equally to this work.

[2]To whom correspondence may be addressed. Email: ccontag@stanford.edu, wenderp@stanford.edu, or waymouth@stanford.edu.

This article contains supporting information online at www.pnas.org/lookup/suppl/doi:10.1073/pnas.1614193114/-/DCSupplemental.

www.pnas.org/cgi/doi/10.1073/pnas.1614193114

which specifically address the delivery challenges posed by the mRNA cargo. These dynamic materials, specifically oligo(carbonate-*b*-α-amino ester)s, function initially as polycations that noncovalently complex, protect, and deliver polyanionic mRNA and then subsequently lose their cationic charge through a controlled self-immolative degradation to a neutral small molecule (Fig. 1). Our hypothesis is that this charge alteration reduces or eliminates the chelative electrostatic anion-binding ability of the originally cationic material, thereby facilitating endosomal escape and enabling free mRNA release into the cytosol for translation. We demonstrate the efficacy of these materials to complex, deliver, and release mRNA in multiple lines of cultured cells including primary mesenchymal stem cells and in animal models, via both i.m. and i.v. routes of administration, resulting in robust gene expression.

Results and Discussion

Design, Synthesis, and Characterization. Organocatalytic ring-opening polymerization (OROP) is an excellent method for the preparation of functionalized biomaterials. OROP provides expedient access to oligomers of low dispersity, avoids metal contaminants associated with some polymerization methods, provides precise control over chain length by varying the ratio of initiator to monomer, and allows for the incorporation of multiple monomer functionalities through cooligomerization (38–41). We have previously reported the synthesis of poly(α-amino ester)s (Fig. 2, **1**) by the OROP of N-protected morpholin-2-ones (41), which are readily generated in two steps and in >76% yield from commercially available diethanolamine. Ring opening of the cyclic morpholinone monomers can be initiated with a primary alcohol under organocatalytic conditions to yield oligo(α-amino ester)s. A global Boc-deprotection affords cationic and water-soluble oligo(α-amino ester) **1**. Unlike the more commonly studied poly(β-amino ester)s (42, 43), as the pH is raised toward basic conditions the oligo(α-amino ester)s rapidly degrade in <5 min through a remarkably controlled and novel sequence of ester-to-amide isomerizations that are exploited here to facilitate mRNA release by loss of electrostatic interactions (Fig. 2*A*).

Our initial mechanistic investigations of this degradation are consistent with the partial deprotonation of the initial ammonium cations, leading to an intramolecular cyclization of the resulting amine into the backbone ester through a five-membered transition state (Fig. 2*A*). The nitrogen of the adjacent monomer unit then engages in a second cyclization through a six-membered transition state to form diketopiperazine **2,** the dimer of a known metabolite (hydroxyethyl glycine) of the Maillard reaction (44). Although slow at low pH, this rearrangement is exceptionally fast and efficient at pH 7.4; homooligomers degrade with a half-life of 2 min (*SI Appendix*, Fig. S1). The unique reactivity of this system can be explained by complementary activation of the backbone ester carbonyl by inductive and hydrogen-bonding interactions that proceed concurrently with carbonyl-assisted deprotonation of the amine cation to produce the required nucleophilic amine. This could involve a stepwise process or it could be concerted with addition to the proximate carbonyl, resulting in either case in an initial ammonium (charged) to amide (neutral) functional group transformation. The resultant hydroxyethylamide is then positioned to engage in a facile six-membered ring cyclization to form diketopiperazine **2**. The unique physical property change (from charged amine to neutral amide) associated with this system represents a potentially broadly exploitable concept for polyanionic drug and probe delivery because charge-altering, -reversing, or -neutralizing systems offer a broad range of concepts for polyanion complexation and delivery with release dictated by a change in physical properties.

Previous work on nucleic acid delivery has highlighted the importance of lipophilic domains on delivery vehicles to facilitate cargo binding and membrane interaction leading to cellular internalization (46–48). This requirement is readily addressed with our living OROP approach, because both lipophilic and charged blocks can be incorporated without additional synthetic steps. For this study, dansyl alcohol initiator **3** was first reacted with dodecyl ester carbonate monomer **5**, and the resulting oligomer, without isolation, was then used to initiate reaction with N-Boc morpholinone monomer **6**, providing amphipathic diblock oligomers consisting of a lipidated oligocarbonate block and a cationic, self-immolative α-amino ester block after deprotection.

An attractive aspect of this technology is that the performance of the cooligomer construct can be tuned using different monomers and block lengths. A small series of oligomeric CARTs of varying lengths and compositions was synthesized by ring opening of dodecyl carbonate **5**, followed by addition and oligomerization of morpholinone **6** (Fig. 2*B* and *SI Appendix*, Fig. S2). CART cooligomers containing an average of 13 lipid units and 11 cationic units (D_{13}:A_{11} **7**), 18 lipid and 17 cationic units (D_{18}:A_{17} **8**), and a homooligomer of 13 cationic units (A_{13} **9**) were synthesized using this strategy. Importantly, each new transporter was prepared in only two steps (oligomerization and deprotection), a combined process requiring only a few hours.

The charge-altering degradation of oligo(carbonate-*b*-α-amino ester)s was analyzed by gel permeation chromatography (GPC). To verify that the rearrangement reaction affects only the cationic domain of amphipathic CARTs while leaving the lipophilic domain intact, two model oligomers were synthesized using pyrenebutanol 4 as a UV-active initiator. Homooligomer pyrene-D_{15} **10** was synthesized and used as a macroinitiator to prepare diblock pyrene-D_{15}:A_{12} **11a**, which was subsequently deprotected to **11b** (Fig. 3*A*). Diblock **11b** was treated with pH 7.4 PBS to effect rearrangement. After 1 h, the solution was concentrated and analyzed by GPC (Fig. 3*B*). The GPC trace of the resultant oligomer **11c** (black) was then compared with protected diblock **11a** (red) and homooligomer **10** (blue). As expected, the GPC traces of the protected **11a** (red, 6.4 kDa) show higher molecular weight than homooligomer **10** (blue, 4.6 kDa). GPC analysis of cationic diblock **11b** after exposure to pH 7.4 PBS showed a diminished molecular weight (4.3 kDa) that was nearly identical to the homooligomer **10** (4.6 kDa), suggesting, in line with the

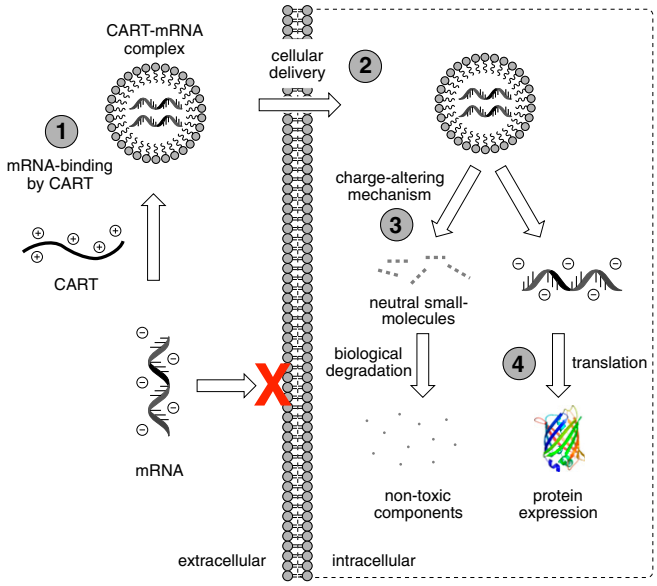

Fig. 1. CARTs effect the complexation (1), intracellular delivery (2), and cytosolic release (3) of mRNA transcripts, resulting in induction of protein expression (4).

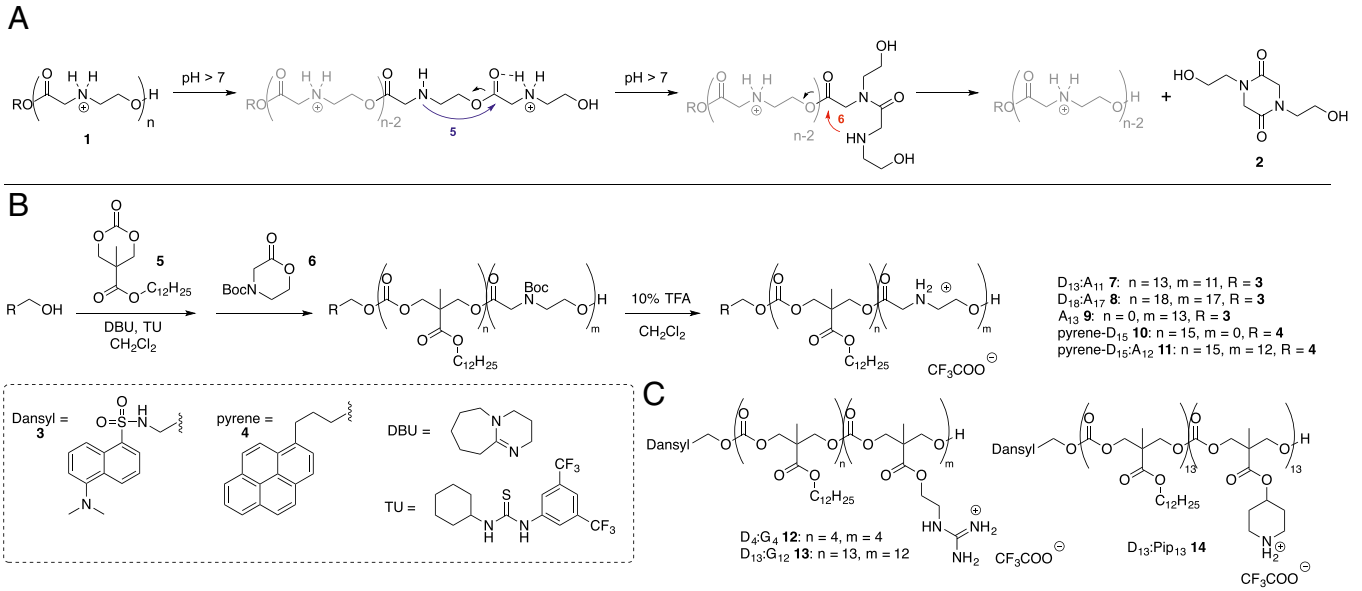

Fig. 2. Oligo(carbonate-*b*-α-amino ester) CARTs designed for mRNA delivery. (*A*) Proposed rearrangement mechanism for oligo(α-amino ester)s through tandem five-membered then six-membered transition states. (*B*) Two-step synthesis of amphipathic oligo(carbonate-*b*-α-amino ester) CARTs via OROP of cyclic carbonate and ester monomers. (*C*) Nonimmolative oligo(carbonate) control compounds synthesized via previously-reported OROP methodology (45, 46).

proposed mechanism, that at physiological pH the cationic portion of the CART degrades whereas the lipophilic block remains intact.

CART-Mediated mRNA Delivery to Cultured Cells. To evaluate the efficacy of CARTs as mRNA delivery vehicles, mRNA encoding EGFP was selected as an optical reporter gene. Flow cytometry analysis of EGFP fluorescence following mRNA delivery allows for simultaneous quantification of the mean protein expression as well as the fraction of cells exhibiting above-baseline levels of fluorescence (percent transfection). Gene expression following treatment of cells with CART/mRNA complexes was compared with expression obtained with EGFP mRNA complexes made with the commercial agent Lipofectamine 2000 (Lipo), as well as two guanidinium-containing compounds known to be effective for siRNA delivery (D_4:G_4 **12** and D_{13}:G_{12} **13**) (46). When HeLa cells were treated with mRNA formulated with Lipo, modest levels of EGFP expression were observed (Fig. 4*A*), but only ∼50% of the cells exhibited fluorescence (Fig. 4*B*). In stark contrast, the oligo (carbonate-*b*-α-amino ester) CART, D_{13}:A_{11} **7**, afforded excellent EGFP expression with >99% transfection efficiency and high mean fluorescent intensity. A second CART with longer block lengths (D_{18}:A_{17} **8**) provided high transfection efficiency (>90%) but lower mean transfection values. Complexes formed with α-amino ester homooligomer A_{13} **9** induced no EGFP expression, consistent with our prior work on amphipathic oligocarbonates for which a hydrophobic domain was necessary for siRNA delivery (46). Contrasting their efficacy in delivering siRNA, complexes formed with guanidinium-functionalized oligocarbonates D_4:G_4 **12** and D_{13}:G_{12} **13** resulted in no detectable EGFP expression. Relative to the rapid self-immolative rearrangement ($t_{1/2}$ = 2 min) of CARTs, oligocarbonates **12** and **13** degrade slowly by passive hydrolysis ($t_{1/2}$ = 8–12 h) (46, 49), establishing a strong correlation between transporter degradation rate and mRNA expression. Collectively, the exceptional performance of the CARTs is consistent with our initial hypothesis that endosomal escape and cytosolic mRNA release can be attributed to the rapid charge-altering transformation of cationic amines to neutral amides.

To study the influence of charge ratios on CART **7** performance, the ratio of cationic oligomer to anionic mRNA was varied from 1:1–50:1 (cation:anion) and the resulting EGFP fluorescence determined (Fig. 4*C*). Values are reported as the theoretical charge ratio of ammonium cations to phosphate anions. EGFP mRNA expression showed a roughly parabolic dependence on charge ratio with maximum EGFP fluorescence resulting from complexes formed at a 10:1 charge ratio. All subsequent experiments were conducted using this optimized ratio. HeLa cells treated with CART/mRNA complexes under these conditions showed no significant decrease in viability (*SI Appendix*, Fig. S3). Additionally, diketopiperizine rearrangement product **2** did not affect cellular viability at concentrations up to 500 μM, well above the 9 μM maximum concentration achieved through self-immolative rearrangement of CART complexes (*SI Appendix*, Fig. S3). Epifluorescence microscopy corroborates flow cytometry

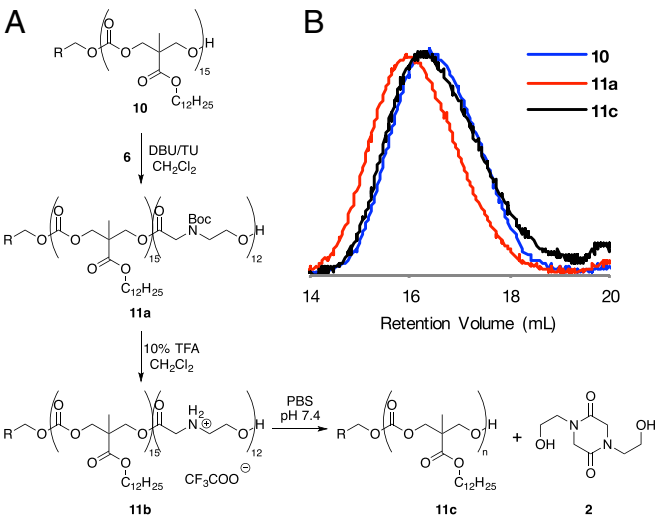

Fig. 3. Exploration of the CART rearrangement mechanism. (*A*) Self-immolative rearrangement of the α-amino ester portion of a block cooligomer yields the intact oligocarbonate block and small molecule **2**. (*B*) GPC traces of D_{15} homooligomer **10** (blue), protected block cooligomer D_{15}:A_{12} **11a** (red), and the product of deprotection and rearrangement **11c** (black). R denotes **4**.

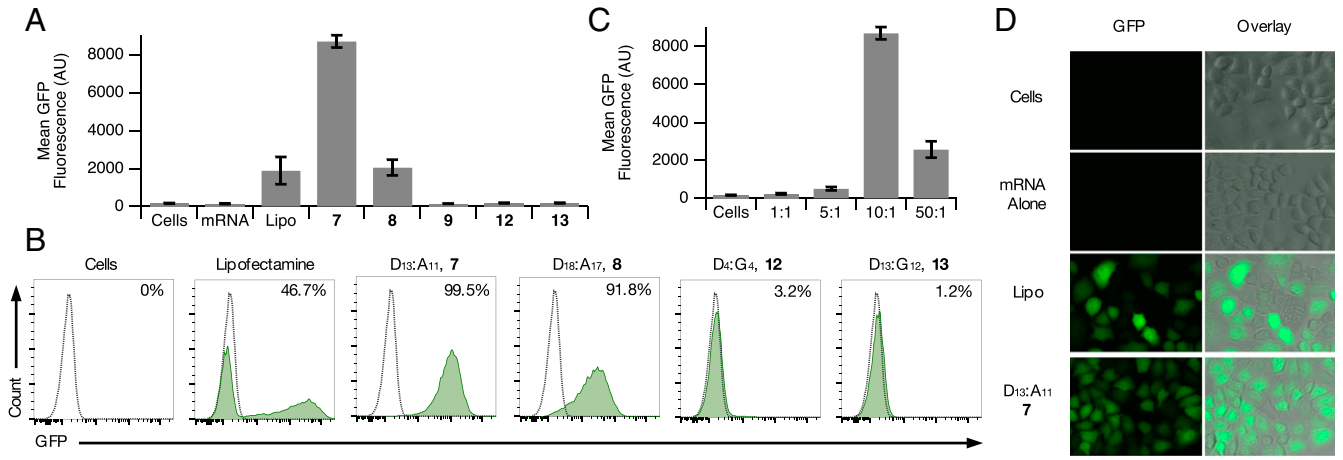

Fig. 4. Evaluation of CARTs for EGFP mRNA delivery. (*A*) Flow cytometry-determined mean EGFP fluorescence intensity from HeLa cells treated with naked mRNA, a Lipo/mRNA complex, and mRNA complexes of transporters **7**–**13**. (*B*) Representative flow cytometry histograms of EGFP fluorescence showing percent transfection in HeLa cells treated with EGFP mRNA complexes. (*C*) The effect of theoretical cation:anion charge ratio on EGFP expression using D_{13}:A_{11} **7** complexes. (*D*) Epifluorescence microscopy images showing EGFP fluorescence alone and a bright-field overlay of HeLa cells treated with mRNA either alone, complexed with Lipo, or complexed with **7**. All data shown are for HeLa cells treated with mRNA concentrations of 125 ng per well in 24-well plates for 8 h. All error bars expressed as ± SD, $n = 3$.

results (Fig. 4*D*), where >92% of HeLa cells treated with the CART/mRNA polyplexes exhibited EGFP fluorescence, whereas <55% of HeLa cells treated with Lipo exhibited EGFP fluorescence.

Characterization of CART Complexes. A series of experiments was conducted to understand how the immolative rearrangement of oligo(carbonate-*b*-α-amino ester) CARTs affects mRNA polyplex formation. Under analogous conditions to those used for cellular transfection, dynamic light scattering (DLS) was used to analyze CART D_{13}:A_{11} **7** and polyelectrolyte complexes formed between **7** and EGFP mRNA. At pH 5.5, the hydrodynamic diameter of the resulting polyplexes was 254 ± 10 nm (*SI Appendix*, Fig. S4*A*). When these polyplexes were added to cell media a change in hydrodynamic diameter from 254 nm to 512 nm occurred over 2 h. In line with our studies on CART rearrangement, the observed increase in size reflects degradative rearrangement of a fraction of the cationic α-amino ester blocks of **7** to the diketopiperazine **2** and the neutral oligocarbonate lipid domain, consistent with aggregation of these segments. When the CART/mRNA complexes are added to unbuffered water, sizes remain at 257 ± 24 nm over the full 2-h experiment (*SI Appendix*, Fig. S4*A*), consistent with previous observations that α-amino ester homooligomers do not rearrange under these conditions (41). Zeta potential measurements are in line with particle size data, with surface charge starting at + 33 ± 7 mV and evolving to – 30 ± 3 mV over 2 h (*SI Appendix*, Fig. S4*B*). This is again consistent with the cationic ammoniums rearranging to neutral amides, leaving the surface predominantly anionic due to the associated oligonucleotide. Interestingly, the differences in rates of rearrangement for the homooligomer (minutes) and the mRNA polyplexes (hours) reflect a complexation-dependent increase in stability of the α-amino ester materials in buffered aqueous environments, putatively by decreasing the rate of deprotonation and thus rearrangement. This enables CART/mRNA complexes to remain stable over therapeutically relevant timescales at pH 7.4 before intracellular degradation.

The size of the formulated polyplexes was not cargo-dependent. When polyplexes were formed with luciferase (Fluc) mRNA, which is approximately twice the length of EGFP (Fluc = 1929 nt vs. EGFP = 996 nt), and added to cell media at pH 7.4, the polyplexes exhibited the same behavior as those formed with EGFP mRNA, suggesting that CART-enabled delivery could be general, working with a variety of mRNA sizes.

Mechanism of Uptake and Release. We further explored the mechanisms of intracellular mRNA delivery and the importance of mRNA release by oligo(carbonate-*b*-α-amino ester) CARTs. Using a Cy5-labeled EGFP mRNA we determined that the mechanism of cell entry for CART **7**/mRNA polyplexes is predominantly endocytic by comparing cellular uptake at 4 °C, a condition known to inhibit endocytotic processes, to normal uptake at 37 °C. Consistent with the expected endocytotic mechanism for ∼250-nm particles, HeLa cells displayed a significant (85%) reduction in Cy5 fluorescence at 4 °C (Fig. 5*A*).

Cellular uptake and mRNA translation following treatment with CART/mRNA polyplexes were then directly compared with polyplexes formed with nonimmolative oligomers. By delivering a mixture of EGFP mRNA and Cy5-labeled EGFP mRNA, analysis of mRNA internalization and expression can be decoupled and simultaneously quantified; Cy5 fluorescence indicates internalized mRNA, irrespective of localization, and EGFP fluorescence denotes cytosolic release and subsequent expression of mRNA. We used this method to explore the effect of backbone structure and cation type by comparing the cellular uptake and mRNA expression of two oligomers to CART D_{13}:A_{11} **7**: nonimmolative, guanidinium-containing D_{13}:G_{12} **13** and nonimmolative, ammonium-containing D_{13}:Pip_{13} **14**.

Cy5-mRNA polyplexes formed with **7**, **13**, or **14** were added to HeLa cells and evaluated by flow cytometry. Although all cooligomers afford similar levels of mRNA uptake, as quantified by Cy5 fluorescence (Fig. 5*B*), only charge-altering D_{13}:A_{11} **7** induces detectable EGFP mRNA expression. These data indicate that all three mRNA polyplexes are internalized by cells efficiently, but without a rapidly degrading backbone the nonimmolative polyplexes derived from **13** and **14** either never escaped the endosome or did not release mRNA on a timescale necessary to enable detectable levels of translation. The lack of EGFP expression by complexes formed with ammonium-containing D_{13}:Pip_{13} **14** further suggests that the efficacy of **7** is not simply due to the difference in electrostatic binding affinity of ammonium vs. guanidinium cations. Rather, the specific, controlled loss of cationic charge through rearrangement is crucial for efficacy. The efficiency of release is likely responsible for differences in mRNA expression using CART **7** and CART **8**, because these CARTs also result in similar uptake of an optically tagged Cy5 mRNA (*SI Appendix*, Fig. S5).

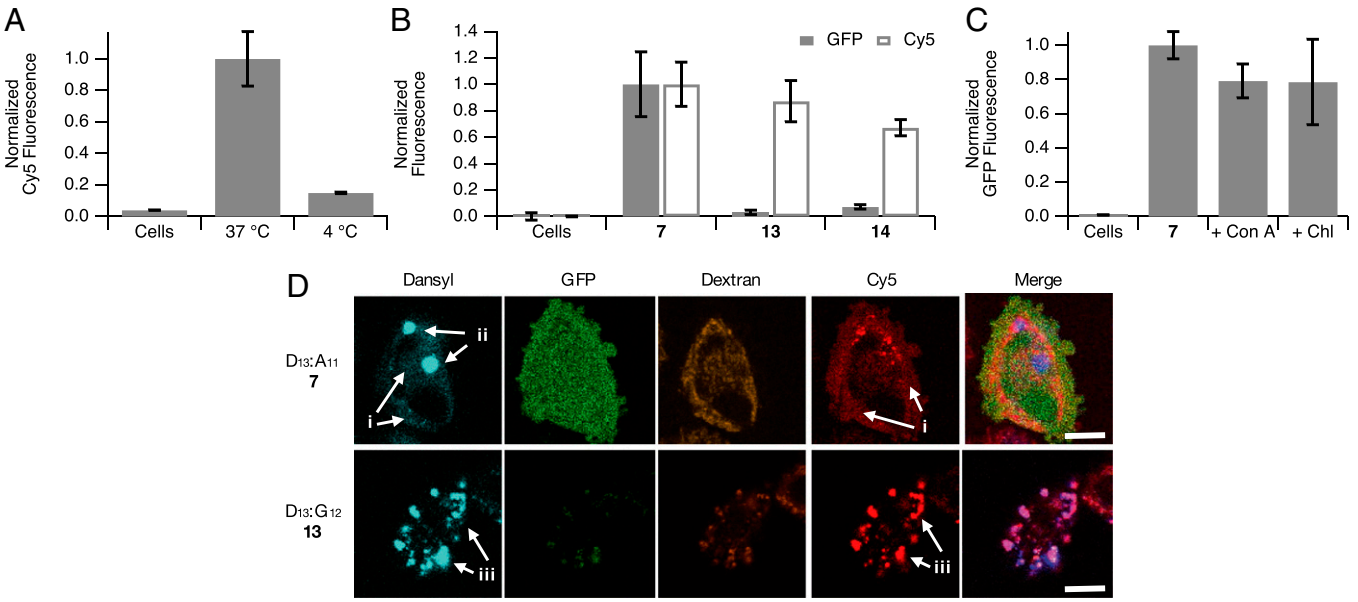

Fig. 5. Functional delivery of mRNA is due to the charge-altering, self-immolative mechanism that drives mRNA release and endosomal escape by CART D_{13}:A_{11} **7**. (*A*) Uptake of CART/Cy5-mRNA complexes at 4 °C, a condition that inhibits endocytosis. (*B*) Relative uptake and expression of Cy5-EGFP mRNA following treatment with complexes formed with degrading and nondegrading transporter systems. Filled bars represent EGFP expression and open bars represent Cy5 fluorescence. (*C*) Effect of endosomal acidification inhibitor (Con A) or endosomolytic agent (Chl) on EGFP expression following CART/mRNA delivery. (*D*) Confocal microscopy of HeLa cells treated with Cy5-mRNA complexes using CART **7** or nonimmolative oligomer **13** after 4 h. Cells were cotreated TRITC-$Dextran_{4400}$. All error bars expressed as ± SD, $n = 3$. (Scale bar, 10 μm.)

In addition to the loss of electrostatic mRNA binding due to the charge-altering, self-immolation mechanism we reasoned that the simultaneous release of the small molecule **2** is also likely to facilitate endosomal escape. To examine this, HeLa cells were cotreated with CART/EGFP mRNA complexes and two compounds known to influence the endosomal microenvironment: concanamycin A (Con A) and chloroquine (Chl). Con A is a specific V-ATPase inhibitor that prevents endosomal acidification (50). Other reports of cationic ammonium-containing materials such as cationic lipid nanoparticles (51, 52) and polyethyleneimine (PEI) (53) have shown 10- to 200-fold decreases in gene delivery when treated with V-ATPase inhibitors due to decreased endosomal buffering and osmotic rupture by the presumed proton sponge effect (54). However, the fluorescence intensity of HeLa cells treated with polyplexes derived from α-amino ester CART **7** is nearly unaffected by treatment with Con A (Fig. 5*C*, 21% decrease, $P = 0.177$), indicating that endosomal acidification and buffering is not necessary to achieve endosomal escape or gene expression with CARTs. Chl is a lysosomotropic agent that has been used to improve gene delivery by increasing endosomal buffering and rupture (55). Others have shown that gene delivery materials without buffering functionality, such as methylated PEI, show substantial increases in gene expression when cotreated with Chl (two- to threefold), whereas buffering vectors such as unmodified PEI are unaffected (53). HeLa cells treated with CART/mRNA polyplexes and Chl showed only a slight decrease in fluorescence (22% decrease, $P = 0.469$), suggesting that endosomal escape is not a limiting factor in mRNA delivery by oligo(carbonate-*b*-α-amino ester) CARTs. This is additionally consistent with the proposed escape through osmotic rupture that already occurs as a result of immolation of **7** and formation of **2**.

The importance of CART-mediated mRNA release and endosomal escape compared with an ineffective transporter (D_{13}:G_{12}, **13**) was further confirmed by confocal microscopy with detection of dansylated transporter, Cy5-mRNA, and tetramethylrhodamine (TRITC)-$Dextran_{4400}$, a stain for endosomal compartments. When cells were imaged 4 h after treatment with CART **7**/Cy5-mRNA complexes diffuse fluorescence was observed for both the Cy5 and dansyl fluorophores, indicating that those materials successfully escaped the endosome and dissociated from the polyplexes (Fig. 5*D*, *i*). The two observed puncta in the dansyl signal (Fig. 5*D*, *ii*) likely arise from some intracellular aggregation of the dansyl-labeled lipidated oligocarbonate blocks, resulting from self-immolative degradation of the cationic segments of CART **7**. Diffuse fluorescence from (TRITC)-$Dextran_{4400}$ is also observed, which can be attributed to endosomal rupture and release of the entrapped dextran. However, when cells are treated with nonimmolative **13**/Cy5-mRNA complexes, both the Cy5 and dansyl fluorescence remain punctate and colocalized (Fig. 5*D*, *iii*). These signals also strongly overlap with punctate TRITC-$Dextran_{4400}$, indicative of endosomal entrapment. Taken together, these data strongly suggest that the charge-altering behavior of CART **7** enables endosomal rupture and mRNA release, contributing to the high performance of these materials for mRNA delivery.

Applications and Animal Experiments. Oligo(carbonate-*b*-α-amino ester) D_{13}:A_{11} **7** was evaluated in additional applications to explore the versatility of CART-mediated mRNA delivery. EGFP mRNA expression following delivery by CART **7** was assayed in a panel of cell lines, including those typically considered to be difficult to transfect (56). In addition to HeLa cells, mRNA expression was compared with that of Lipo in murine macrophage (J774), human embryonic kidney (HEK-293), CHO, and human hepatocellular carcinoma (HepG2) cells by treating with CART complexes formed with EGFP mRNA (Fig. 6*A*). In all cell lines tested the percentage of cells expressing EGFP using the CART **7** was >90%, whereas treatment with Lipo induced expression in only 22–55% of the cells. Importantly, this suggests that this delivery system is general for a variety of human and nonhuman cell types. In addition to immortalized cell lines, mRNA expression was also observed in primary CD1 mouse-derived mesenchymal stem cells (MSCs) with high transfection efficiency.

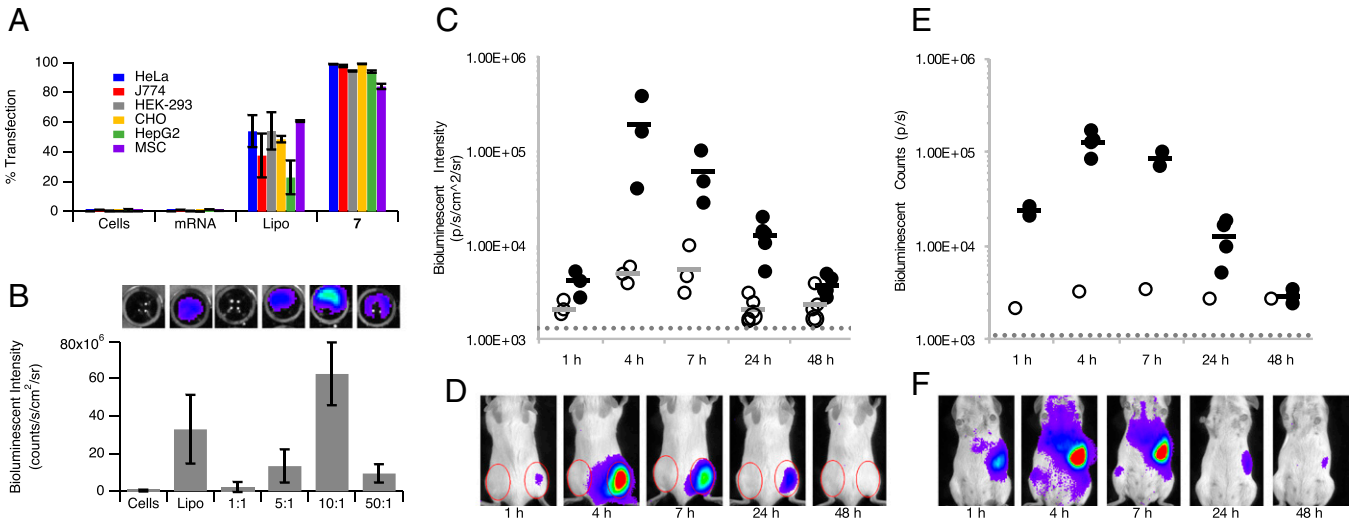

Fig. 6. Applications of mRNA delivery using CARTs in multiple cell lines and mice. (*A*) Transfection efficiencies of EGFP mRNA delivery by D_{13}:A_{11} **7** compared with Lipo in HeLa (blue), J774 (red), HEK 293 (gray), CHO (yellow), and HepG2 (green) cell lines and primary CD1-derived mesenchymal stem cells (purple). Error bars expressed as ± SD, $n = 3$. (*B*) Delivery of Fluc mRNA with CART **7** follows the same trend in charge ratio as EGFP. Charges reported as theoretical (cation:anion) ratios. Representative bioluminescent images for treatment conditions are shown above their corresponding bars. Error bars expressed as ± SD, $n = 3$. (*C*) In vivo BLI following i.m. injection of naked Fluc mRNA (○) and CART/mRNA complexes using **7** (●). Bars represent average of all animals ($n = 3$ at 1, 4, and 7 h; $n = 5$ for 24 and 48 h). (*D*) Representative bioluminescence images following i.m. injection of naked mRNA (left flank) or CART/mRNA complexes (right flank). (*E*) In vivo BLI following i.v. (tail vein) injection of naked mRNA (○) and CART/mRNA complexes (●). Bars represent average of all animals ($n = 2$ for 1 and 7 h; $n = 4$ for 4, 24, and 48 h). Dotted lines are background BLI signals from an animal that had not been injected with D-luciferin. (*F*) Representative BLI images of mice treated with CART/mRNA complexes via i.v. injection.

Not only is the efficiency of CART-mediated delivery consistent across different cell types, but the consistency is also observed using mRNA of different lengths, because we observed that **7** also effectively delivers the larger firefly luciferase (Fluc) mRNA, substantially outperforming Lipo (Fig. 6*B*). Analogous to trends observed with EGFP mRNA, a 10:1 (cation:anion) ratio resulted in the highest level of Fluc bioluminescence, despite the difference in mRNA lengths, indicating that delivery efficiency is largely independent of cargo size. Simultaneous expression of multiple mRNA transcripts was demonstrated by coformulating CART **7**/mRNA complexes with binary mixtures of EGFP and Fluc mRNA (*SI Appendix*, Fig. S6). These polyplexes induce expression of two unique proteins at levels proportional to the mass percent of that transcript in the formulation.

In vivo bioluminescence imaging (BLI) enables localization and quantification of expression following mRNA delivery in living animals (57). To assess the efficacy of CART/mRNA complexes following systemic or local routes of administration, as would be required for vaccination or protein augmentation therapies, we evaluated i.v. and i.m. injections of CART-complexed Fluc mRNA in anesthetized BALB/c mice using BLI. For each mouse, 7.5 μg mRNA was complexed with CART D_{13}:A_{11} **7** and administered by i.m. injection into the right thigh muscle in 75 μL PBS. As a direct control, 7.5 μg of naked mRNA was injected in the opposite flank. D-luciferin was systemically administered i.p. at 15 min before imaging for each time point, and luciferase expression was evaluated over 48 h, starting at 1 h after the administration of mRNA complexes. When Fluc mRNA was delivered with polyplexes derived from **7** into the muscle, high levels of luciferase activity were observed at the site of injection (Fig. 6 *C* and *D*). This expression peaked at 4 h and was still observable after 48 h. In contrast, i.m. injection of naked mRNA afforded only low levels of luciferase expression, as measured by photon flux, in all five mice.

When polyplexes were administered via tail vein injection at the same dose we observed robust abdominal bioluminescence as early as 1 h postinjection, peaking at 4 h (Fig. 6 *E* and *F*). High levels of expression persisted for 24 h, with detectable bioluminescence after 48 h. Bioluminescence is primarily localized in these images to the spleen and liver. No bioluminescent signals were observed when naked mRNA was administered i.v. For all mice studied, there were no outward signs of toxicity observed either immediately after injection or over a period of several weeks following treatment as indicated by ruffled fur, changes in behavior, hunched posture, or death.

The ability to successfully deliver functional mRNA via multiple routes of administration in vivo is critical for developing RNA-based therapeutics. Local i.m. injections are the preferred route of administration for many therapies, including vaccination, due to the ease of administration and ability to access naive dendritic and antigen-presenting cells in the dermal and muscle tissue. Following i.v. injections, the localization of mRNA polyplexes in tissues along the reticuloendothelial system such as the liver or spleen provides many opportunities in inducing immunotherapeutic responses. Spleen localization, as observed with our nontargeted complexes, is particularly exciting for future studies involving mRNA-based immunotherapy due to large numbers of dendritic and immune cells in that tissue. Liver localization was also apparent in these animals, and expression in this tissue may have applicability for treatment of hereditary monogenic hepatic diseases requiring protein augmentation or replacement such as hereditary tyrosinemia type I, Crigler–Najjar syndrome type 1, alpha-1-antityrpsin deficiency, Wilson disease, and hemophilia A and B, or acquired liver diseases such as viral hepatitis A–E and hepatocellular carcinoma (58–60).

Conclusions

We have developed a general, tunable, and step-economical strategy for mRNA delivery that uses unique oligomeric transporters that operate through an unprecedented mechanism to

effectively deliver mRNA into cells and animals with excellent efficiency. Our approach draws on a facile two-step process using OROP and global deprotection to rapidly prepare the oligo(carbonate-*b*-α-amino ester) delivery vehicles. Following intracellular delivery, these CARTs undergo a remarkable intramolecular rearrangement, during which cationic amines are converted to neutral amides, resulting in decomplexation and release of anionic mRNA into the cytosol for translation.

mRNA therapeutics have the potential to transform disease treatment. The clinical implementation of this technology, however, rests on the availability of safe, general, and efficacious delivery methods. We have achieved high levels of gene expression in cultured cells and living animals using mRNA complexed and delivered by CARTs. The effectiveness of mRNA delivery using these CARTs represents a strategy for mRNA delivery that results in functional protein expression in both cells and animals. The success of these materials will enable widespread exploration into their utilization for vaccination, protein replacement therapy, and genome editing, while augmenting our mechanistic understanding of the molecular requirements for mRNA delivery.

Methods

Materials. Reagents were purchased from Sigma-Aldrich and used as received unless otherwise indicated. The 1-(3,5-bis-trifluoromethyl-phenyl)-3-cyclohexyl-thiourea (39), MTC-guanidine monomer (49), MTC-dodecyl monomer **5** (46), MTC-piperidine monomer (45), N-Boc morpholinone monomer **6** (41), and dansyl alcohol **3** (49) were all prepared according to literature procedures. Unless otherwise noted, all commercial solvents and reagents were used without further purification. Methylene chloride (CH_2Cl_2) and tetrahydrofuran (THF) were passed through an alumina drying column (Solv-Tek Inc.) using nitrogen pressure. Petroleum ether, pentane, hexane, ethyl acetate (EtOAc), and methanol (MeOH) were obtained from Fisher Scientific. Deuterated solvents were purchased from Cambridge Isotope Laboratories. Regenerated cellulose dialysis membranes (Spectra/Por 6 Standard RC; molecular weight cutoff 1,000) were purchased from Spectrum Laboratories, Inc.

PBS buffer was prepared from RNase-free 10× PBS solution (Fisher Scientific). DMEM was purchased from Invitrogen and supplemented with 10% FBS and 1% penicillin/streptomycin. Lipofectamine 2000 was purchased from Life Technologies, and 3-(4,5-dimethylthiazol-2-yl)-2,5-diphenyl tetrazolium bromide was purchased from Fluka. Con A was purchased from Santa Cruz Biotechnology.

mRNAs. EGFP mRNA (5meC, Ψ, L-6101), Fluc mRNA (5meC, Ψ, L-6107), and Cy5-EGFP mRNA (5meC, Ψ, L-6402) were purchased from TriLink BioTechnologies Inc.

Instrumentation. Gel permeation chromatography (GPC) was performed in tetrahydrofuran (THF) at a flow rate of 1.0 mL/min on a Malvern Viscotek VE2001 chromatography system equipped with four 5-μm Waters columns (300 × 7.7 mm) connected in series. The Viscotek VE3580 refractive index (RI) and VE3210 UV/Vis detectors and Viscotek GPCmax autosampler were used, and the number average molecular weights (M_n in g·mol^{-1}) and molecular weight distributions (M_w/M_n) were calibrated using monodisperse polystyrene standards (Polymer Laboratories). Particle size was measured by DLS on a Malvern Zetasizer Nano ZS90. Flow cytometry analysis was performed on a BD LSRII FACS Analyzer (Stanford University Shared FACS Facility). Laser scanning confocal microscopy was carried out using a Leica SP8 White Light Confocal microscope with a 40× HC PL APO, CS2 oil objective lens (Stanford University Cell Sciences Imaging Facility). Bioluminescence was measured using a CCD camera (IVIS 100; Xenogen Corp.) and analyzed using Living Image Software (Perkin-Elmer). Epifluorescence microscopy was performed on a Zeiss Axio Observer.Z1 with an X-Cite 120Q wide-field excitation light source and a GFP filter set. Images were acquired with a CoolSNAP HQ^2 camera and transferred to a computer for image analysis.

Cell Lines. HeLa, J774, HepG2, and HEK-293 cells were maintained in DMEM supplemented with 10% (vol/vol) FBS and 1% penicillin/streptomycin. CHO cells were maintained in F12 media supplemented with 10% FBS and 1% penicillin/streptomycin. All cells were grown at 37 °C in a 5% CO_2 atmosphere. Cells were passaged at ~80% confluence.

MSCs were prepared according to the method of Huang et al. (61). Briefly, femurs were excised from two 8-wk-old female CD1 mice, and the tissue was removed from the outside of the bone. The ends of the bones were then cut with a sterile scissors. The marrow was flushed from the four bones with DMEM 10% FCS containing penicillin/streptomycin using a 3-mL syringe and a 25-gauge needle in a 10-cm tissue culture-treated Petri dish. The marrow was disrupted and dispersed by pipetting but not filtered or otherwise manipulated. The dish was incubated for 6 d, whereupon a characteristic monolayer developed. The culture was then washed twice with PBS and trypsinized with 0.25% trypsin (Gibco) for 5 min at 37 °C. The cells were then collected and transferred to a 75-cm^2 tissue culture flask and incubated for 3 d, until 90% confluence was achieved. The culture could be maintained for two more passages, but growth was greatly reduced upon four passages. For transfection, the cells were plated at 1.2×10^4 per well in 24-well plates.

Preparation of Cooligomers D_n:A_m. For the representative synthesis of D_{13}:A_{11} **7**, a flame-dried vial was charged with MTC-dodecyl monomer **5** (33.2 mg, 0.1 mmol), dansyl initiator **3** (3.9 mg, 0.013 mmol), and 50 μL CH_2Cl_2. Diazabicycloundecene (DBU) (0.8 mg, 0.005 mmol) and thiourea catalyst (TU) (Fig. 2*B*) (2.0 mg, 0.005 mmol) in 50 μL CH_2Cl_2 were added to the reaction vial and allowed to stir. After 2 h, N-Boc monomer **6** was added to the vial as a solid and the reaction was allowed to stir for 3 h. After a total of 5 h, the reaction was quenched with five drops of AcOH then concentrated under reduced pressure. The crude material was dialyzed in CH_2Cl_2 against MeOH (1.0-kDa dialysis bag). Concentration afforded 37.9 mg pale green residue. End group analysis (2.8 ppm) by ^{1}H NMR shows DP 13:11.

Procedure for Guanidine and Morpholinone Deprotection. To a vial containing Boc-protected cooligomer (representative scale 0.011 mmol) dissolved in 4.5 mL CH_2Cl_2 was added TFA (0.5 mL). The reaction was sealed under inert atmosphere and stirred at room temperature for 12 h. The solvent was concentrated in vacuo to afford the deprotected cationic cooligomers as oils (>99%). Complete deprotection was confirmed by ^{1}H-NMR analysis.

GPC Degradation Experiment. Cationic D_{15}:A_{12} **11b** (21.0 mg, 0.0027 mmol) in CH_2Cl_2 (1.5 mL) was treated with PBS pH 7.4 (200 μL) and allowed to stir for 1 h. The reaction was then concentrated under reduced pressure, taken up in THF, and sonicated for 5 min. The resulting heterogeneous mixture was filtered through a 0.22-μm syringe filter and submitted for GPC analysis.

Comparing the GPC trace of the homo- (4,600 Da) and diblock (6400 Da) oligomers shows a higher molecular weight of the protected diblock oligomer **11a**. Comparing the homoblock **10** and the degraded diblock oligomer **11c** (4,300 Da) shows overlap of the UV and RI signals matching the homoblock **10** (Fig. 3*B*).

EGFP mRNA Delivery and Expression in HeLa Cells by Flow Cytometry. HeLa cells were seeded at 40,000 cells per well in 24-well plates and allowed to adhere overnight. Oligomer/mRNA polyplexes were prepared by mixing RNase-free PBS pH 5.5 and EGFP mRNA with various amounts of oligomer from DMSO stock solutions, to achieve specific cooligomer/mRNA ratios (optimized to a theoretical cation:anion ratio of 10:1, 8.4 μL total volume). The complexes were incubated for 20 s at room temperature before treatment. The Lipo control was prepared in OptiMEM per the manufacturer's instructions. The cells were washed with serum-free DMEM and mRNA/Lipo solution was added to a final volume of 200 μL per well and 125 ng mRNA per well. After washing with serum-free DMEM, 2.5 μL of the mRNA/cooligomer complexes was added to a total volume of 200 μL, all conditions in triplicate, for a final mRNA concentration of 125 ng per well. The cells were incubated for 8 h at 37 °C then trypsinized with trypsin-EDTA (0.05%) for 10 min at 37 °C. Serum-containing DMEM was added and the contents of each well centrifuged and the supernatant removed, and the pelleted cells were redispersed in PBS (125 μL) and transferred to FACS tubes and read on a flow cytometry analyzer (LSR-II.UV at Stanford University). The data presented are the geometric mean fluorescent signals from 10,000 cells analyzed. For transfection efficiency, untreated cells were gated for no EGFP expression, and the data presented are the percentages of 10,000 cells analyzed with higher EGFP expression than untreated cells. Error is expressed as ± SD. All other cell lines were used as above in their respective media. For HepG2 cells, 5 mM EDTA was added to the PBS used to resuspend the cell pellets for flow cytometry.

Epifluorescence Microscopy. HeLa cells were seeded in black, glass-bottomed, 12-well plates and allowed to adhere overnight. EGFP mRNA polyplexes were prepared as above (final concentration of 125 ng mRNA per well in 400 μL total volume) and added to serum-free DMEM. Cells were incubated for 8 h at 37 °C, then media was removed and 1 mL of DMEM without phenol red was added to wells. GFP fluorescence was acquired using a Zeiss Epifluorescence Microscope with GFP filter set. Percent transfection was

determined by dividing the number fluorescent cells observable in a given field of view by the total number of cells.

DLS and Zeta Potential. mRNA/cooligomer complexes were prepared at a 10:1 (cation:anion) charge ratio as above using 500 ng EGFP mRNA and added to 120 μL RNase-free PBS pH 5.5, 7.4, or neutral RNase-free water. The solution was immediately transferred to a disposable clear plastic cuvette and the size measured. Size measurements were taken at the initial time (1 min) and at 15-min intervals over 2 h. The sizes reported are the z-averages. Zeta potential measurements were taken by diluting the mRNA:cooligomer complexes formulated for DLS into 800 μL water, transferring to zeta cell (DTS1060), and measuring zeta potential. All values reported are the average of a minimum of three trial runs. Error expressed as ± SD.

Mechanism of Cell Entry at 4 °C. For studies at reduced temperature, HeLa cells were incubated in serum-free DMEM at 4 °C for 30 min before treatment with Cy5-EGFP mRNA polyplexes. Polyplexes were prepared as above using Cy5-labeled EGFP mRNA at a final concentration of 125 ng mRNA per well in 200 μL. The cells were treated on ice and incubated for 1 h at 4 °C and directly compared with cells treated at 37 °C by flow cytometry. The fold difference in fluorescence was calculated from the mean Cy5 fluorescence of cells treated at 4 °C divided by the mean Cy5 fluorescence of cells treated at 37 °C.

Fluorescent Cy5-EGFP mRNA Delivery and Expression Analysis. To measure cellular uptake and release of oligomer/mRNA polyplexes, HeLa cells were treated with polyplexes prepared as above using Cy5-labeled EGFP mRNA at a final concentration of 62.5 ng mRNA per well. Cells were prepared and analyzed by flow cytometry for both EGFP and Cy5 fluorescence as above.

Effect of Endosomal Inhibitors on EGFP mRNA Expression. To measure the effect of inhibiting endosomal acidification, Con A was added to HeLa cells treated with CART **7**/EGFP mRNA polyplexes (125 ng mRNA per well, prepared as above) at final concentration of 50 nM. Chl was added to HeLa cells treated with CART **7**/mRNA polyplexes at a final concentration of 100 μM. Cells were prepared and analyzed by flow cytometry for EGFP fluorescence as above.

Confocal Microscopy. HeLa cells were seeded in an eight-chambered glass-bottomed dish (Nunc Lab-Tek II; Thermo Scientific) at 10,000 cells per well and allowed to adhere overnight. Before treatment, cells were washed with serum-free DMEM, and 200 μL of serum-free DMEM with 100 μM TRITC-Dextran (average molecular weight 4,400; Sigma) was added to each well. Cy5-EGFP mRNA polyplexes were prepared as above (final concentration of 125 ng mRNA per well) and added to each corresponding well. Cells were incubated for 4 h at 37 °C, then media was removed and 500 μL of PBS containing 10 mM Hepes buffer solution was added. Cells were imaged using a Leica SP8 White Light Confocal microscope tuned for DAPI (dansyl), GFP, DsRed (TRITC-Dextran), and Cy5.

BLI of Fluc mRNA Delivery to HeLa Cells. HeLa cells were seeded at 10,000 cells per well in black 96-well plates and allowed to adhere overnight. mRNA polyplexes and Lipo control were prepared as above using Fluc mRNA (final concentration of 50 ng mRNA per well in 50 μL total volume). All conditions were performed in replicates of six. Cells were incubated with treatment for 8 h at 37 °C, then medium was removed and 100 μL of a D-luciferin solution (300 μg/mL) in DMEM was added to the cells. The resultant luminescence was measured using an IVIS 50 or IVIS 200 (Xenogen product line; Perkin-Elmer) CCD camera and Living Image Software. Data represent the average of three experiments with error expressed as ± SD.

BLI of Fluc mRNA Delivery in Female BALB/c Mice. Fluc mRNA expression was analyzed in female BALB/c mice with an IVIS 200 system (Xenogen product line; Perkin-Elmer), located in the Stanford Center for Innovation in In-Vivo Imaging. Animals were anesthetized with isoflurane using an SAS3 anesthesia system (Summit Anesthesia Support) and an EVAC 4 waste gas evacuation system (Universal Vaporizer Support).

For i.v. administration, 7.5 μg of Fluc mRNA was injected into the tail vein of each mouse in 75 μL PBS. mRNA was either administered naked or in complexation with CART **7** at a 10:1 cation:anion ratio. For i.m. injections, CART/mRNA complexes of 7.5 μg Fluc mRNA were injected into the right flank of each mouse in 75 μL PBS. A control dose of naked Fluc mRNA was administered in the same volume to the left flank of the mouse.

Expression of Fluc was analyzed by BLI after i.p. injecting D-luciferin at 150 mg/kg. A grayscale body surface reference image (digital photograph) was taken under weak illumination. After switching off the light source, photons emitted from luciferase-expressing cells within the animal body and transmitted through the tissue were quantified over a defined period ranging up to 5 min using the software program Living Image (Perkin-Elmer). For anatomical localization, a pseudocolor image representing light intensity (blue, least intense; red, most intense) was generated in Living Image and superimposed onto the grayscale reference image. Experimental protocols were approved by the Stanford Administrative Panel on Laboratory Animal Care.

ACKNOWLEDGMENTS. We thank Prof. Lynette Cegelski for materials, tissue culture equipment, and use of a plate reader and epifluorescence microscope; Prof. Chaitan Khosla for use of HeLa cells; and Prof. Richard Zare for materials and the use of the Malvern Zetasizer DLS. This work was supported by Department of Energy Grant DE-SC0005430 and National Science Foundation Grant NSF CHE-1306730 (to R.M.W.) and NIH Grants NIH-CA031841 and NIH-CA031845 (to P.A.W.). This work was also funded in part through a generous gift from the Chambers Family Foundation for Excellence in Pediatric Research (to C.H.C.) and the Child Health Research Institute at Stanford University (to C.H.C.). Support through the Stanford Center for Molecular Analysis and Design (C.J.M.) and through fellowships from the National Science Foundation (J.R.V.) is also acknowledged. Flow cytometry data were collected on an instrument in the Stanford Shared FACS Facility obtained using NIH S10 Shared Instrument Grant S10RR027431-01. Confocal microscopy was collected on an instrument in the Stanford Cell Sciences Imaging Facility supported by National Center for Research Resources Award 1S10OD010580.

1. Sahin U, Karikó K, Türeci Ö (2014) mRNA-based therapeutics–Developing a new class of drugs. *Nat Rev Drug Discov* 13(10):759–780.
2. McIvor RS (2011) Therapeutic delivery of mRNA: The medium is the message. *Mol Ther* 19(5):822–823.
3. Kranz LM, et al. (2016) Systemic RNA delivery to dendritic cells exploits antiviral defence for cancer immunotherapy. *Nature* 534(7607):396–401.
4. Chahal JS, et al. (2016) Dendrimer-RNA nanoparticles generate protective immunity against lethal Ebola, H1N1 influenza, and Toxoplasma gondii challenges with a single dose. *Proc Natl Acad Sci USA* 113(29):E4133–E4142.
5. Yin H, et al. (2016) Therapeutic genome editing by combined viral and non-viral delivery of CRISPR system components in vivo. *Nat Biotechnol* 34(3):328–333.
6. Vallazza B, et al. (2015) Recombinant messenger RNA technology and its application in cancer immunotherapy, transcript replacement therapies, pluripotent stem cell induction, and beyond. *Wiley Interdiscip Rev RNA* 6(5):471–499.
7. Kreiter S, Diken M, Sahin U (2014) mRNA vaccination and personalized cancer therapy. *Cancer Immunotherapy Meets Oncology*, eds Britten CM, Kreiter S, Diken M, Rammensee H-G (Springer, Berlin), pp 89–100.
8. Whitehead KA, Langer R, Anderson DG (2009) Knocking down barriers: Advances in siRNA delivery. *Nat Rev Drug Discov* 8(2):129–138.
9. Pack DW, Hoffman AS, Pun S, Stayton PS (2005) Design and development of polymers for gene delivery. *Nat Rev Drug Discov* 4(7):581–593.
10. Putnam D (2006) Polymers for gene delivery across length scales. *Nat Mater* 5(6):439–451.
11. Tezgel AÖ, et al. (2013) Novel protein transduction domain mimics as nonviral delivery vectors for siRNA targeting NOTCH1 in primary human T cells. *Mol Ther* 21(1):201–209.
12. Lee JB, Hong J, Bonner DK, Poon Z, Hammond PT (2012) Self-assembled RNA interference microsponges for efficient siRNA delivery. *Nat Mater* 11(4):316–322.
13. Luo D, Saltzman WM (2000) Synthetic DNA delivery systems. *Nat Biotechnol* 18(1):33–37.
14. Kauffman KJ, Webber MJ, Anderson DG (2016) Materials for non-viral intracellular delivery of messenger RNA therapeutics. *J Control Release* 240:227–234.
15. Yin H, et al. (2014) Non-viral vectors for gene-based therapy. *Nat Rev Genet* 15(8):541–555.
16. Tavernier G, et al. (2011) mRNA as gene therapeutic: How to control protein expression. *J Control Release* 150(3):238–247.
17. Sharova LV, et al. (2009) Database for mRNA half-life of 19 977 genes obtained by DNA microarray analysis of pluripotent and differentiating mouse embryonic stem cells. *DNA Res* 16(1):45–58.
18. Islam MA, et al. (2015) Biomaterials for mRNA delivery. *Biomater Sci* 3(12):1519–1533.
19. Bettinger T, Carlisle RC, Read ML, Ogris M, Seymour LW (2001) Peptide-mediated RNA delivery: A novel approach for enhanced transfection of primary and post-mitotic cells. *Nucleic Acids Res* 29(18):3882–3891.
20. Schlake T, Thess A, Fotin-Mleczek M, Kallen K-J (2012) Developing mRNA-vaccine technologies. *RNA Biol* 9(11):1319–1330.
21. Habrant D, et al. (2016) Design of ionizable lipids to overcome the limiting step of endosomal escape: Application in the intracellular delivery of mRNA, DNA, and siRNA. *J Med Chem* 59(7):3046–3062.
22. Rejman J, Tavernier G, Bavarsad N, Demeester J, De Smedt SC (2010) mRNA transfection of cervical carcinoma and mesenchymal stem cells mediated by cationic carriers. *J Control Release* 147(3):385–391.

23. Gonçalves C, Akhter S, Pichon C, Midoux P (2016) Intracellular availability of pDNA and mRNA after transfection: A comparative study among polyplexes, lipoplexes, and lipopolyplexes. *Mol Pharm* 13(9):3153–3163.
24. Kübler H, et al. (2015) Self-adjuvanted mRNA vaccination in advanced prostate cancer patients: A first-in-man phase I/IIa study. *J Immunother Cancer* 3(1):26.
25. Weide B, et al. (2009) Direct injection of protamine-protected mRNA: Results of a phase 1/2 vaccination trial in metastatic melanoma patients. *J Immunother* 32(5): 498–507.
26. Rittig SM, et al. (2011) Intradermal vaccinations with RNA coding for TAA generate CD8+ and CD4+ immune responses and induce clinical benefit in vaccinated patients. *Mol Ther* 19(5):990–999.
27. Cheng C, Convertine AJ, Stayton PS, Bryers JD (2012) Multifunctional triblock copolymers for intracellular messenger RNA delivery. *Biomaterials* 33(28):6868–6876.
28. Uzgün S, et al. (2011) PEGylation improves nanoparticle formation and transfection efficiency of messenger RNA. *Pharm Res* 28(9):2223–2232.
29. Nuhn L, Kaps L, Diken M, Schuppan D, Zentel R (2016) Reductive decationizable block copolymers for stimuli-responsive mRNA delivery. *Macromol Rapid Commun* 37(11): 924–933.
30. Uchida S, et al. (2013) In vivo messenger RNA introduction into the central nervous system using polyplex nanomicelle. *PLoS One* 8(2):e56220.
31. Uchida H, et al. (2014) Modulated protonation of side chain aminoethylene repeats in N-substituted polyaspartamides promotes mRNA transfection. *J Am Chem Soc* 136(35):12396–12405.
32. Crowley ST, Poliskey JA, Baumhover NJ, Rice KG (2015) Efficient expression of stabilized mRNA PEG-peptide polyplexes in liver. *Gene Ther* 22(12):993–999.
33. Fenton OS, et al. (2016) Bioinspired alkenyl amino alcohol ionizable lipid materials for highly potent in vivo mRNA delivery. *Adv Mater* 28(15):2939–2943.
34. Li B, et al. (2015) An orthogonal array optimization of lipid-like nanoparticles for mRNA delivery in vivo. *Nano Lett* 15(12):8099–8107.
35. Kauffman KJ, et al. (2015) Optimization of lipid nanoparticle formulations for mRNA delivery in vivo with fractional factorial and definitive screening designs. *Nano Lett* 15(11):7300–7306.
36. Brito LA, et al. (2014) A cationic nanoemulsion for the delivery of next-generation RNA vaccines. *Mol Ther* 22(12):2118–2129.
37. Matsui A, Uchida S, Ishii T, Itaka K, Kataoka K (2015) Messenger RNA-based therapeutics for the treatment of apoptosis-associated diseases. *Sci Rep* 5:15810.
38. Dove AP, Pratt RC, Lohmeijer BGG, Waymouth RM, Hedrick JL (2005) Thiourea-based bifunctional organocatalysis: Supramolecular recognition for living polymerization. *J Am Chem Soc* 127(40):13798–13799.
39. Pratt RC, et al. (2006) Exploration, optimization, and application of supramolecular thiourea–amine catalysts for the synthesis of lactide (co)polymers. *Macromolecules* 39(23):7863–7871.
40. Kamber NE, et al. (2007) Organocatalytic ring-opening polymerization. *Chem Rev* 107(12):5813–5840.
41. Blake TR, Waymouth RM (2014) Organocatalytic ring-opening polymerization of morpholinones: New strategies to functionalized polyesters. *J Am Chem Soc* 136(26): 9252–9255.
42. Lynn DM, Langer R (2000) Degradable poly(β-amino esters): Synthesis, characterization, and self-assembly with plasmid DNA. *J Am Chem Soc* 122(44):10761–10768.
43. Green J, Zugates G, Langer R, Anderson D (2009) Poly(beta-amino esters): Procedures for synthesis and gene delivery. *Methods Mol Biol* 480:53–63.
44. Requena JR, et al. (1997) Carboxymethylethanolamine, a biomarker of phospholipid modification during the maillard reaction in vivo. *J Biol Chem* 272(28):17473–17479.
45. Pratt RC, Nederberg F, Waymouth RM, Hedrick JL (2008) Tagging alcohols with cyclic carbonate: A versatile equivalent of (meth)acrylate for ring-opening polymerization. *Chem Commun (Camb)* (1):114–116.
46. Geihe EI, et al. (2012) Designed guanidinium-rich amphipathic oligocarbonate molecular transporters complex, deliver and release siRNA in cells. *Proc Natl Acad Sci USA* 109(33):13171–13176.
47. Wender PA, Huttner MA, Staveness D, Vargas JR, Xu AF (2015) Guanidinium-rich, glycerol-derived oligocarbonates: A new class of cell-penetrating molecular transporters that complex, deliver, and release siRNA. *Mol Pharm* 12(3):742–750.
48. deRonde BM, et al. (2016) Optimal hydrophobicity in ring-opening metathesis polymerization-based protein mimics required for siRNA internalization. *Biomacromolecules* 17(6):1969–1977.
49. Cooley CB, et al. (2009) Oligocarbonate molecular transporters: Oligomerization-based syntheses and cell-penetrating studies. *J Am Chem Soc* 131(45):16401–16403.
50. Huss M, et al. (2002) Concanamycin A, the specific inhibitor of V-ATPases, binds to the V(o) subunit c. *J Biol Chem* 277(43):40544–40548.
51. Khalil IA, Kogure K, Akita H, Harashima H (2006) Uptake pathways and subsequent intracellular trafficking in nonviral gene delivery. *Pharmacol Rev* 58(1):32–45.
52. Bartz R, et al. (2011) Effective siRNA delivery and target mRNA degradation using an amphipathic peptide to facilitate pH-dependent endosomal escape. *Biochem J* 435(2): 475–487.
53. Akinc A, Thomas M, Klibanov AM, Langer R (2005) Exploring polyethylenimine-mediated DNA transfection and the proton sponge hypothesis. *J Gene Med* 7(5): 657–663.
54. Kichler A, Leborgne C, Coeytaux E, Danos O (2001) Polyethylenimine-mediated gene delivery: A mechanistic study. *J Gene Med* 3(2):135–144.
55. Erbacher P, Roche AC, Monsigny M, Midoux P (1996) Putative role of chloroquine in gene transfer into a human hepatoma cell line by DNA/lactosylated polylysine complexes. *Exp Cell Res* 225(1):186–194.
56. Zhang X, Edwards JP, Mosser DM (2009) The expression of exogenous genes in macrophages: Obstacles and opportunities. *Methods Mol Biol* 531:123–143.
57. Contag CH, Bachmann MH (2002) Advances in in vivo bioluminescence imaging of gene expression. *Annu Rev Biomed Eng* 4(1):235–260.
58. Nguyen TH, Ferry N (2004) Liver gene therapy: Advances and hurdles. *Gene Ther* 11(Suppl 1):S76–S84.
59. Nguyen TH, Ferry N (2007) Gene therapy for liver enzyme deficiencies: What have we learned from models for Crigler-Najjar and tyrosinemia? *Expert Rev Gastroenterol Hepatol* 1(1):155–171.
60. Suda T, et al. (2009) Progress toward liver-based gene therapy. *Hepatol Res* 39(4): 325–340.
61. Huang S, et al. (2015) An improved protocol for isolation and culture of mesenchymal stem cells from mouse bone marrow. *J Orthopaedic Trans* 3(1):26–33.